A Pharmacodynamic Analysis of Choroidal Neovascularization in a Porcine Model Using Three Targeted Drugs

Jeffrey Tran,[1] Caroline Craven,[1] Kathy Wabner,[1,2] Jenn Schmit,[1,2] Brock Matter,[3] Uday Kompella,[3] Hans E. Grossniklaus,[1] and Timothy W. Olsen[1]

[1]Emory Eye Center, Emory University Department of Ophthalmology, Atlanta, Georgia, United States
[2]The University of Minnesota, Department of Civil, Environmental, and Geo-Engineering, Minneapolis, Minnesota, United States
[3]The University of Colorado, Department of Pharmaceutical Sciences, University of Colorado School of Pharmacy, Aurora, Colorado, United States

Correspondence: Timothy W. Olsen, Mayo Clinic, 200 First Street SW, Rochester, MN 55905, USA; olsen.timothy@mayo.edu.

Submitted: December 2, 2016
Accepted: June 21, 2017

Citation: Tran J, Craven C, Wabner K, et al. A pharmacodynamic analysis of choroidal neovascularization in a porcine model using three targeted drugs. *Invest Ophthalmol Vis Sci*. 2017;58:3732–3740. DOI:10.1167/iovs.16-21230

Purpose. To compare the efficacy of microneedle-delivered suprachoroidal (SC) pazopanib to intravitreal (Ivit) delivery of pazopanib, bevacizumab, or a fusion protein hI-con1 versus vehicle controls on choroidal neovascularization (CNV) growth in a pig model.

Methods. Forty-one pigs were injected on the day of CNV induction (hI-con1 on postinduction day 14) with either 2.5 mg Ivit bevacizumab ($n = 9$), 1 mg Ivit pazopanib ($n = 9$), 300 Ivit μg hI-con1 ($n = 4$), or 1 mg SC pazopanib ($n = 9$), vs. 10 vehicle controls (3 SC + 7 Ivit = 10). Pigs were euthanized at week 2 (11), 3 (8), 4 (11), and 8 (11), and eyes were fixed for histology. The size of the CNV was determined from histology, and CNV height was the primary outcome measure. Immunostaining for cytotoxic T-cells was performed in the hI-con1 study.

Results. In 39 of 41 (95%) eyes, type 2 CNV lesions were identified. One CNV lesion was lost during dissection. One animal was euthanized due to surgical complications. For mean CNV size comparisons, Ivit pazopanib had smaller mean height measurements (90 ± 20 μm) versus controls (180 ± 20 μm; $P = 0.009$), and Ivit pazopanib had smaller maximum CNV height (173 ± 43 μm) compared to SC pazopanib (478 ± 105 μm; $P = 0.018$). The mean lesion size in hI-con1–treated animals trended smaller than in controls ($P = 0.11$). Immunostaining did not detect cytotoxic T-cells.

Conclusions. Intravitreal pazopanib and to a lesser extent hI-con1 reduced the size of CNV lesions. The pig model has nearly a 100% rate of type 2 CNV induction and is a reliable preclinical model with pharmacodynamics similar to humans.

Keywords: choroidal neovascularization, intravitreal drug delivery, porcine

Subretinal choroidal neovascularization (CNV) in the macula is a known complication of end-stage age-related macular degeneration (AMD). The goal of this in vivo preclinical study was to optimize pharmacodelivery to the macula using a well-documented pig model of CNV.[1–6] AMD is a leading cause of irreversible blindness in those over age 60 from developed countries.[7] Furthermore, neovascular AMD (nAMD) has been effectively managed in many patients by using agents that target the vascular endothelial growth factor (VEGF) protein. Using a preclinical large animal study, we sought to determine the best and most effective pharmacologic management of pathologic CNV by examining strong candidate drugs. Drug delivery was either by intravitreal (Ivit) injection or into the suprachoroidal space (SCS) using a microneedle delivery system.[8]

Surgically induced CNV in the pig is a reliable and reproducible model that has been extensively studied and is well characterized in the literature.[1–6] In general, fibrovascular growth extends through surgically induced defects in Bruch's membrane followed by debridement of the retinal pigment epithelium (RPE) that leads to subretinal CNV, subretinal fluid accumulation, hemorrhage, scaring, and fibrosis.[5] While not specifically an aging model, the pig model has relevance for preclinical pharmacologic studies due to the anatomic similarities between a pig and a human eye. Key parallels include eye size, choroidal blood flow, retinal pigment epithelial characteristics, and scleral thickness.[9]

Ranibizumab, afilbercept, and the off-label use of bevacizumab are commonly used VEGF inhibitors, each demonstrating therapeutic efficacy in treating nAMD.[10–13] Lassota et al.[2] demonstrated that Ivit bevacizumab treatments led to a reduction in vascular endothelial cells as well as fluorescein leakage in the pig model of CNV. In humans, treatment demands of Ivit delivery require frequent injections, thus creating a tremendous burden for patients and their care providers,[14] and also creating an added burden to the health care system.[15] Endophthalmitis, cataract, retinal detachment, and retinal pigment epithelial rips are all uncommon, yet represent meaningful, potential risks with each injection.[16,17]

There are several drug delivery systems and sustained-release formulations that are currently in various stages of investigation. Delivery routes include Ivit, transscleral,[18] and suprachoroidal (SC).[19–21] The ideal drug and route depends

Table 1. Study Design

	Study	Week 2	Week 3	Week 4	Week 8
Pazopanib SC	$N = 9$	3		3	3
Pazopanib Ivt	$N = 8$	3		2	3
Bevacizumab Ivt	$N = 9$	3		3	3
hI-con1 Ivt	$N = 4$		2	2	
Controls	$N = 10$	2	2	4	2

A total of 41 pigs were enrolled and 40 completed the study (one was euthanized for surgical complications). Pigs were treated on the day of induction of choroidal neovascularization. The hI-con1 first day of treatment was postoperative day 14. All groups were compared to vehicle-treated controls.

largely upon the underlying disease state, the agent being delivered, the target tissue, and the local pharmacokinetics. For example, SC drug delivery bypasses transscleral diffusion and may selectively target the choroidal tissue or the RPE.[20,21] Gilger et al.[22] demonstrated that a lower dose of corticosteroid delivered through the SCS was as effective as a higher Ivit dose at reducing inflammation in a porcine model.

In an earlier study, we described a novel system for SC drug delivery using a flexible cannula with a fiberoptic illumination system that localizes delivery in the pig model.[20] This system was used to access the SCS and demonstrated sustained-release pharmacokinetics of triamcinolone with very low drug levels in the systemic circulation. However, studies in the pig model of SC bevacizumab delivery demonstrated rapid clearance from the SCS when compared to the Ivit route.[23] Hollow microneedles represent another method to gain access to the SCS.[24] Particles of different size can be delivered to the SCS by changing the microneedle length and the infusion pressure.[25]

Pazopanib is a drug that has been reported to inhibit both VEGF pathways and the platelet-derived growth factor receptor-B (PDGFR-B) in mice, thus could represent an excellent candidate antiangiogenic agent that also has a theoretic potential to induce vessel regression.[26–28] Due to the relative solubility and molecular size, pazopanib likely has pharmacokinetics similar to triamcinolone acetonide and fluocinolone acetonide. Pazopanib is a small molecule (MWt = 437.5) with a very low solubility and may have a favorable dissolution-controlled, sustained pharmacokinetic profile from both the vitreous and SCS. Oral pazopanib has been shown to suppress CNV in a mouse model.[28] However, the topical delivery of pazopanib in human subjects did not demonstrate a meaningful therapeutic clinical result in the treatment of CNV.[29,30]

The hI-con1 is a human immune conjugate fusion protein that combines a protein composed of a mutated factor VII conjugated to the Fc domain of human IgG1 immunoglobin that binds to tissue factor (TF) and has been studied in tumor biology.[31] Currently in phase 1/2 clinical trials, hI-con1 is a chimeric antibody with a high affinity for TF and activates a potent immune response through recruitment of natural killer (NK) cells and complement leading to cytolysis of CNV in mouse models.[31–33] TF is expressed on endothelial cells and is located on CNV but not on normal vessels.[34] A study published by Bora et al.[35] demonstrated that mice injected with either the hI-con1 protein or an adenoviral vector expressing this protein significantly reduced CNV formation in a laser-induced mouse model of CNV. Tezel et al.[36] have shown that hI-con1 binds to the endothelium of CNV in a pig model.

In the present study, we used the pig CNV model to compare the efficacy of several novel anti-VEGF agents in combination with selected drug delivery routes. We used microneedles to deliver pazopanib into the SCS and compared this to Ivit delivery of either pazopanib, bevacizumab, or hI-con1 with appropriate vehicle controls.

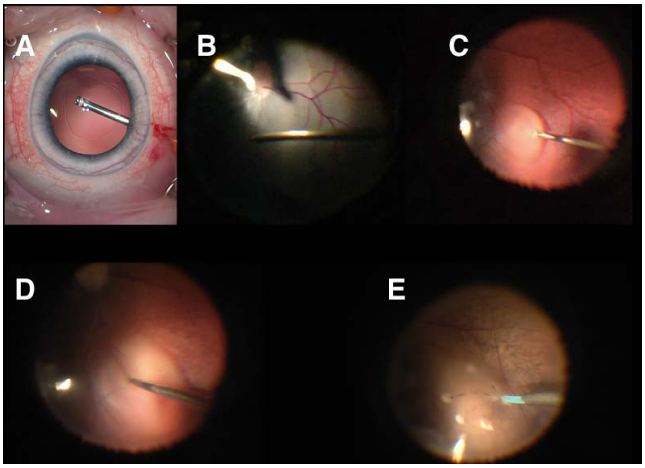

Figure 1. Steps for surgical induction of choroidal neovascularization in the pig eye. (**A**) Standard three-port pars plana vitrectomy with lensectomy. (**B**) An illuminated pick (*left*) combined with aspiration from a soft-tip silicone cannula (*right*) are used simultaneously to elevate and detach the adherent posterior hyaloid to a region just peripheral to the vascular arcades. (**C**) A 27-gauge cannula with tubing connected to the viscous injection system of the vitrectomy machine is used to inject balanced salt solution (BSS) and create a retinal detachment in the area centralis. (**D**) A 23-gauge micro-vitreoretinal (MVR) blade is used to puncture Bruch's membrane. Five to seven punctures are performed in a circular pattern equivalent to the area of the optic disc with the infusion-controlled intraocular pressure (IOP) set at 90 mm Hg. (**E**) A soft-tip silicone cannula is used to aspirate the retinal pigment epithelial cells and bleeding from around each puncture site. The IOP is slowly decreased back to 35 mm Hg, and small areas of subretinal hemorrhage from the punctures are common.

Materials and Methods

All animal studies were performed with permission from the Institutional Animal Care and Use Committee (IACUC) at Emory University and in accordance with the guidelines on conduct of animal experiments and experimental design in keeping with the ARVO Statement for the Use of Animals in Ophthalmic and Vision Research.

Induction of CNV and Drug Delivery

The right eyes of 41 pigs were operated, and the groups are summarized in Table 1. After general sedation, eyes were dilated using a combination of atropine (1%) and phenylephrine (2.5%). Animals were placed on nasal oxygen (4 L/min) and a warming blanket (37°C) and were carefully monitored with a pulse oximeter and rectal temperature probe throughout the procedure. Body temperature was maintained at 37°C. The pig head was positioned on a conforming pillow to optimize surgical exposure and stability.

CNV was induced using minimal modification of a published procedure in the pig model described by Lassota et al.[4] and Kiilgaard et al.[6] The surgical steps are summarized in Figures 1A to 1E. A 23-gauge pars plana lensectomy and vitrectomy was performed followed by elevation of the posterior hyaloid to a region just anterior to the vascular arcades, followed by a core vitrectomy. The retina was detached in the area centralis (macular equivalent in the pig) using an infusion of balanced salt solution (BSS; Alcon Laboratories, Fort Worth, TX, USA) through a 27-gauge cannula

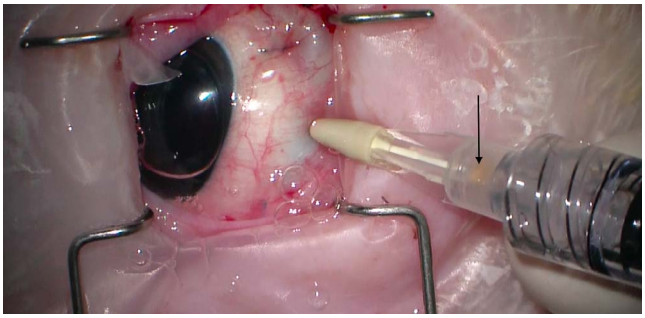

FIGURE 2. Surgical photograph of the microneedle with a pazopanib suspension being injected into the suprachoroidal space of an air-filled, aphakic pig eye following induction of CNV. The syringe is oriented perpendicular to the sclera with the entry site measured 6 mm posterior to the limbus. There is sufficient scleral indentation for the tip of the microneedle to reach the suprachoroidal space (SCS) while smooth, easy plunger advancement ensures that delivery is into the SCS (resistance indicates intrastromal scleral injection). Note also that there is yellow pazopanib suspension remaining at the needle hub (*black arrow*). The majority of the suspension was visibly passing into the SCS.

connected by tubing to the variable infusion pressure–controlled viscous fluid injection system of the vitrectomy machine (Accurus, Alcon Laboratories). Intraocular pressure was increased to approximately 90 mm Hg; Bruch's membrane was punctured using a 23-gauge micro-vitreoretinal (MVR) blade at approximately five to seven sites to approximate the size of the optic nerve. Thus, all CNV lesions were created with a similar two-dimensional area. Next, a soft-tip cannula was extended into the subretinal space, and the RPE cells along with any associated hemorrhage were gently aspirated from around each Bruch's puncture site. The intraocular pressure was slowly returned to approximately 35 mm Hg. Small hemorrhages at the puncture site were common. An air–fluid exchange was completed, and the sclerotomies, conjunctiva, and sclera were sutured using 7-0 Vicryl suture (Ethicon, Cincinnati, OH, USA). All attempts were made to maintain an intraocular pressure of at least 20 mm Hg during globe closure in order to minimize the risk of subretinal hemorrhage and the secondary influences that such hemorrhages induce. Drug groups were randomly assigned and revealed to the surgeon only after CNV induction in order to minimize possible bias.

One pig was euthanized at the time of surgery due to a severe intraoperative hemorrhagic complication. Thus, on the day of surgery, pigs ($n = 40$) were each given a 100-µm injection of either 2.5 mg Ivit bevacizumab ($n = 9$), 1 mg Ivit pazopanib ($n = 8$), 1 mg SC pazopanib ($n = 9$), or a vehicle control ($n = 10$). All 10 control animals had either a pars plana Ivit or transscleral SC injection of vehicle control using either a 30-gauge needle (Ivit) or microneedle (SC; $n = 7$ and 3, respectively, for 10 total controls; Table 1).

Pazopanib was purchased from Cell Signaling Technology, Inc. (Danvers, MA, USA), and the material within the container was sterilized using gamma-irradiation. Pazopanib was suspended in sterile BSS and a viscoelastic material (ProVisc, Alcon Laboratories) to achieve a final concentration of 2 mg/mL. Pazopanib particles were crushed with a sterile 18-gauge needle in a microfuge container, essentially a mortar and pedestal mechanical approach, and vortex mixed well over 5 minutes. Then, the suspension was subjected to forceful and aggressive turbulence using a back-and-forth mixing through a three-way stopcock connecting two dual syringes. Particle size was not quantified.

A 1100-µm (length) 30-gauge microneedle (donated by Clearside Biomedical, Inc., Alpharetta, GA, USA) was used to deliver either 1 mg pazopanib or vehicle control into the SCS. During the 100-µL SC injections (Fig. 2), the needle was carefully directed perpendicularly (90°) to the sclera 6 mm posterior to the limbus. Low resistance on the syringe plunger confirmed successful delivery into the SCS.

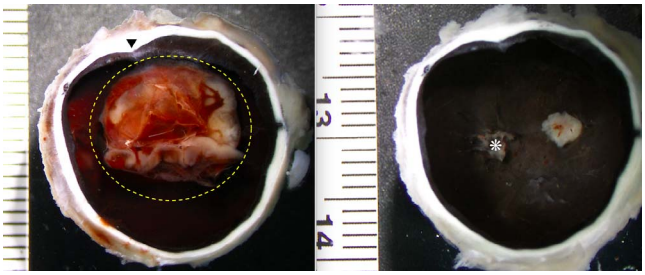

FIGURE 3. Gross dissection. (**A**) Transection of the anterior segment (*black arrowhead* at the edge of cut sclera) exposing the detached retina (outlined with a *yellow dashed circle*), old hemorrhage (red in color), and whitish proliferative vitreoretinopathy. (**B**) After dissection of the neurosensory retina, the bare retinal pigment epithelium, the optic nerve (*right*), and the choroidal neovascular lesion (*white dashed circle*) are visible.

Factor VII Conjugate Fusion Protein: hI-con1

We used the same pig model for CNV induction and identical methodology as described above. Importantly, the initial and only injection was delivered on postoperative day 14. The Ivit injection of either 300 µg/0.1 mL hI-con1 ($n = 4$) or vehicle (control, $n = 4$) was performed using a 30-gauge needle. The delayed injection was performed in order to compare CNV lesion size of treated eyes with controls and assess for possible CNV regression. Animals were examined with color fundus photos and fluorescein angiograms and then enucleated on postoperative week 3 ($n = 4$, 2 treated and 2 control) and week 4 ($n = 4$, 2 treated and 2 control). The eyes were studied with histopathology and fluorescence immunohistochemistry using anti-CD31, anti-CD56, anti-CD105, anti-CD3, and anti-CD68 antibodies directed to NK cells, T-cells, and macrophages.

All animals were euthanized using a phenobarbital solution (390 mg/mL). Right eyes were enucleated on postoperative week 2, 3, 4, and 8 following CNV induction and immediate treatment (Table 1). Eyes were immediately fixed in 10% formalin and processed for histopathology. The anterior segments were removed from each eye using a sharp blade, exposing the posterior segments (Fig. 3). The detached retina was carefully dissected with forceps and scissors to aid in visualizing the CNV induction site. The posterior pole was photographed. Eyes were then embedded into paraffin blocks and sectioned in a pupil–optic nerve (PO) manner to include the area centralis (macular equivalent) and optic nerve. Serial 7-µm step sections were prepared, numbered sequentially, and mounted on glass slides. For each eye, 50 to 250 slides were available. In the hI-con1 study, sections were also stained with antibody to CD31, CD56, CD105, CD3, and CD68 following a confirmatory positive control for T-cells, NK cells, and macrophages using sections from spleen tissue.

CNV Evaluation

During the first eye gross dissection, the CNV complex was inadvertently removed with the detached retina. Subsequently, we carefully separated the CNV and found that it was present in all of the remaining 40 globes. The CNV lesion size was assessed and quantified using previously described histopathologic measurements and mapping techniques and was done

Investigative Ophthalmology & Visual Science

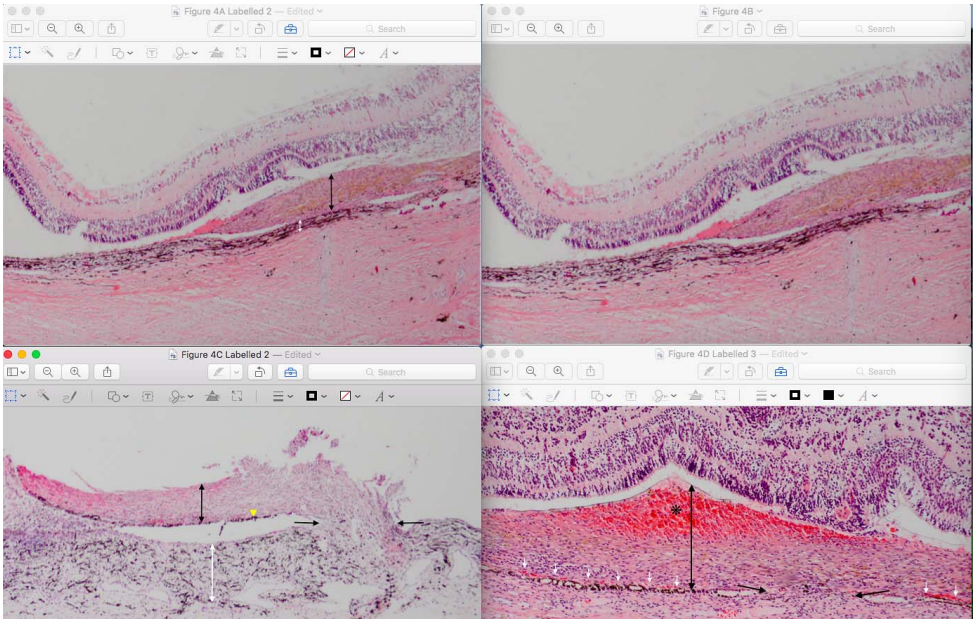

Figure 4. Histopathology of type 2 choroidal neovascularization (CNV). (**A**) A low-power, ×10 hematoxylin and eosin (H&E) micrograph with a partially detached retina and an underlying type 2 CNV (*black double arrow*) sitting on the choroid (*white double arrow*). (**B**) A ×10 H&E micrograph of CNV (*black double arrow*) extending through the surgically induced break in Bruch's membrane (*black arrows*), from the underlying choroid (*white double arrow*) and secondary reactive retinal pigment epithelial (RPE) hyperplasia (*yellow arrowheads*) growing on the undersurface of the CNV. (**C**) A higher-power ×25 H&E micrograph of subretinal CNV (*black double arrow*), endothelial lined vascular channels (*white arrows*), a defect in Bruch's membrane (*black arrows*), and subretinal hemorrhage (*black asterisk*).

in a masked fashion.[37] Lesion height, as described in the natural history of CNV in the pig model by Lassota et al.,[3] was determined to be the primary measure of effect, and it should also be noted that this lesion height changed very little in measures taken more than 14 days post induction.[3] We rely on lesion height at multiple postoperative time intervals as the key variable to assess treatment effect in this model (all enucleation time-point data within each group are pooled for the final analysis).

Histopathology Mapping

Slides were examined using light microscopy (Olympus BH2, Tokyo, Japan) equipped with a standard measuring reticule calibrated to the ×2, ×4, ×10, and ×40 objectives for reference lengths. Specimens were examined to localize the optic nerve, retinal detachment, and any visible breaks in Bruch's membranes. Photographs were taken using the Olympus DP12 camera.

To assess the size and extent of the induced CNV, a reticule was used to measure cross-sectional CNV width (X). Most importantly, CNV height (Z) was measured at the thickest section. To capture the CNV length (Y), we recorded the slide numbers and number of consecutive serial sections. In the hI-con1 study, greatest dimensional pixel area from the histology images was quantified, three measures per globe, using a software image analysis program (Adobe Illustrator CS6v16; San Jose, CA, USA).

Systemic Pazopanib Drug Levels

The serum levels of pazopanib in each pig were measured from 5 mL blood obtained at the time of euthanasia. Samples were transferred on ice and centrifuged for 15 minutes at 2400*g* at 4°C in a refrigerated centrifuge (Beckman Coulter GS-6R with the GH3.8 rotor; Indianapolis, IN, USA). Next, 1.0-mL aliquots were drawn from each and frozen (–80°C).

Statistical Analysis

A 1-way ANOVA and unpaired Student's *t*-test was used to assess for meaningful CNV lesion size from the observations and measurements (StataCorp LP, College Station, TX, USA). A P value of ≤ 0.05 was used to identify statistically significant groups. We constructed a mixed linear model of the measurements as a function of treatment with a random intercept per animal.

Results

CNV Induction

In 39 of 41 pigs (95%), we confirmed the presence of type 2 CNV with histopathology (Fig. 4). We suspect that CNV was present in all 40 eyes, yet we cannot confirm one case. The other animal had a severe intraoperative massive hemorrhagic retinal detachment and was euthanized prior to recovery. Most animals had postoperative lid edema, mild corneal edema, and conjunctival injection that healed within 1 week. One animal in the Ivit pazopanib group required systemic antibiotics for a postoperative fever. Other complications are summarized in Table 2. In addition, subretinal hemorrhages were common in this model, yet difficult to quantify. Postoperatively, we tried to

Table 2. Complications Observed During Gross Pathologic Review

	Retinal Detachment	Vitreous Hemorrhage
Pazopanib SC	8	0
Pazopanib Ivt	5	0
Bevacizumab Ivt	9	2
Controls	4	1

Partial, funnel, and full retinal detachments were observed and are shown in the retinal detachment column.

Table 3. Choroidal Neovascular Membrane Lesion Measurements

	Maximum Height, Z max	Mean Height, Z avg	Surface Area, mm², X × Y	Volume, mm³, X × Y × Z	Area in Pixels², X × Y
Pazopanib SC	478 ± 105 μm	147 ± 33 μm	0.28 ± 0.04	0.15 ± 0.03	
Pazopanib Ivit	173 ± 43 μm	90 ± 20 μm	0.24 ± 0.11	0.15 ± 0.08	
Bevacizumab Ivit	348 ± 123 μm	146 ± 37 μm	0.24 ± 0.07	0.11 ± 0.03	
hI-con1					58,018 ± 37,884
Controls	650 ± 267 μm	180 ± 20 μm	0.36 ± 0.15	0.13 ± 0.03	192,740 ± 65,888

Z max = lesion height, measured from Bruch's membrane to the maximum measured height of the choroidal neovascular membrane (CNV). The Z avg is the average height taken from multiple measurements of lesion height along the length of the histology section of greatest horizontal diameter (5–10). These measurements were derived from differing time points following CNV induction. Thus, the data are consolidated as our goal was to determine the maximum lesion height at any postoperative point.

maintain a constant intraocular pressure and avoid hypotony, a condition that would lead to more subretinal bleeding. Due to the need for repeat anesthesia, assessment of postoperative subretinal blood was not performed.

Suprachoroidal Delivery Using Microneedles

Delivering pazopanib using the microneedle (Fig. 2) was efficient and simple. Small, unquantifiable, yet visible particulate elements of the poorly soluble drug clustered at a turbulent flow portion at the connection of the syringe and needle shaft, so the delivered dose was probably less than the calculated dose.

Histopathology for CNV Lesion Size Evaluation

Following removal of the anterior segments (Fig. 3), retinal detachments, vitreous hemorrhage, and proliferative fibrosis were commonly observed. The key histologic features (Fig. 4) demonstrate type 2 CNV lesion growing through breaks in Bruch's membrane, under the neurosensory retina, and with the presence of reactive RPE proliferation over the surface of the CNV. The maximum heights (shown graphically) reached significance, while the mean height (average of multiple measurements taken at 5 to 10 intervals along the course of the histopathology slide that had the greatest horizontal diameter), surface area, and calculated volumes did not reach statistical significance (Table 3; Fig. 5). In the Ivit hI-con1 group as compared to vehicle control, the average pixel area size of the hI-con1–treated CNV lesions (58,018 ± 37,884 pixels²) was smaller than that of control CNV lesions (192,740 ± 65,888 pixels², $P = 0.11$). The vehicle-treated control CNV lesions were visibly thicker than in the hI-con1–treated eyes (Fig. 6). The color fundus photograph of an animal at postsurgical week 3, postinjection week 1 along

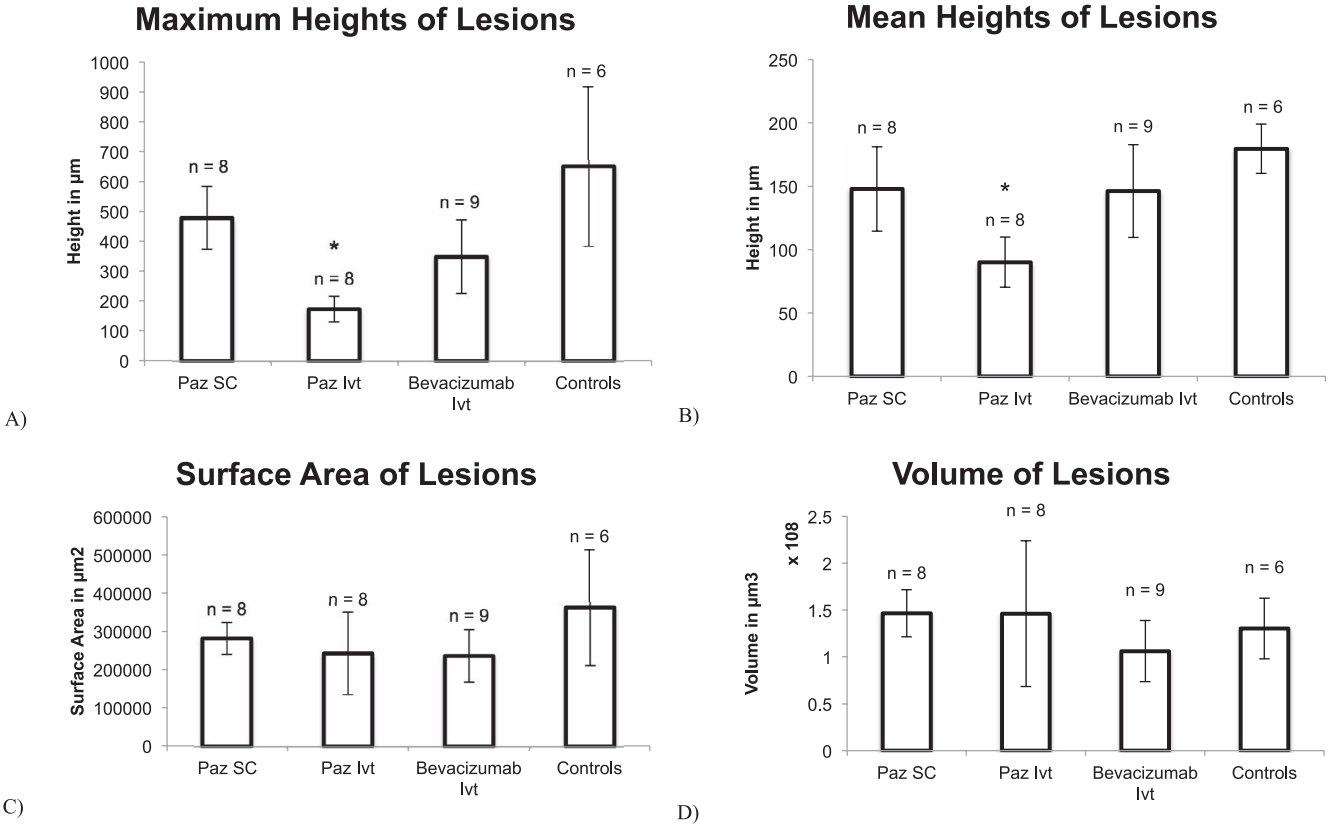

Figure 5. Choroidal neovascular size (*statistically significant, $P < 0.05$). **(A)** Comparison of maximum lesion height with standard error (SE) bars (n = number of animals per group). **(B)** Mean lesion height as measured by taking the average of multiple measures across the greatest diameter of each CNV lesion.

Investigative Ophthalmology & Visual Science

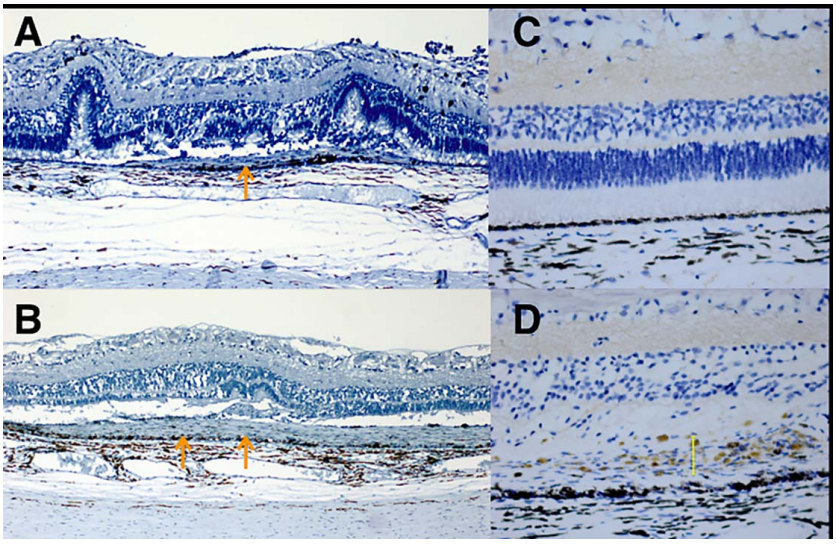

Figure 6. Histopathology of type 2 choroidal neovascularization (CNV). **(A)** A 25× toluidine blue stain of a hI-con1–treated, partially regressed CNV (*orange arrow*) on underlying choroidal tissue. **(B)** A 25× toluidine blue stain of the vehicle CNV (*orange double arrow*) on underlying choroidal tissue (*red double arrow*). The vehicle-treated control CNV lesions are consistently thicker than in the hI-con1–treated eyes. **(C)** A 100× hI-con1–treated CNV with negative staining of anti-CD56 for NK cells. **(D)** A 100× vehicle CNV with positive staining of anti-CD56 (*brown cells* marked by *yellow bracket*).

with the corresponding fluorescein angiogram, is shown in Figure 7.

The maximum CNV height of the Ivit pazopanib-treated eyes (173 ± 43 μm) was significantly smaller than in the SC pazopanib group (478 ± 105 μm; $P = 0.018$) and smaller than in the controls (650 ± 268 μm; $P = 0.06$) (Fig. 5A). The maximum CNV height in the Ivit bevacizumab group (348 ± 123 μm) was only marginally less than in the SC pazopanib group and controls ($P = 0.44$ and $P = 0.27$, respectively). The mean Ivit pazopanib CNV height (90 ± 20 μm) was smaller than in the SC pazopanib-treated eyes (148 ± 33 μm; $P = 0.15$) and significantly smaller than in the controls (180 ± 20 μm; $P = 0.009$). There was only a marginal decrease in the mean height of lesions for the Ivit bevacizumab group (146 ± 37 μm) compared to controls (180 ± 20 μm; $P = 0.49$; see Fig. 5B).

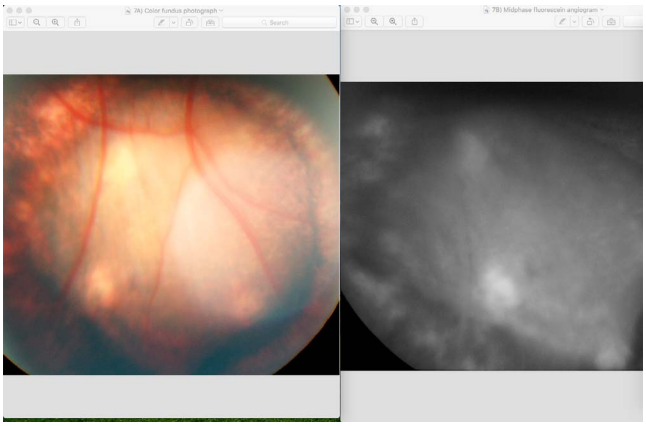

Figure 7. Clinical images. *Left*: color fundus photograph of the postoperative appearance on postoperative week 3 of the subretinal choroidal neovascularization (CNV) in the pig model with reactive retinal pigment epithelium (RPE). *Right*: midphase fluorescein angiogram of the CNV demonstrating hyperfluorescence, especially at the puncture sites and some blocking defect from overlying reactive hyperplasia of the overlying RPE.

There were no meaningful differences in CNV surface area measurements in any group. The CNV surface area measures from the Ivit bevacizumab (0.24 ± 0.07 mm^2), the SC pazopanib (0.28 ± 0.04 mm^2), and Ivit pazopanib (0.24 ± 0.11 mm^2) groups did not reach statistical significance ($P = 0.41$, $P = 0.57$, and $P = 0.52$, respectively) when compared to controls. Similarly, in 13 of 32 CNV volume calculations, there were no significant differences between any groups when compared to the relevant control group.

In the subgroup comparing IVit injection of hI-con1 to vehicle control, the average pixel area size of the hI-con1–treated CNV lesions (58,018 ± 37,884 $pixels^2$) was smaller than for control CNV lesions (19,2740 ± 65,888 $pixels^2$, $P = 0.11$, Fig. 5C). The vehicle-treated control CNV lesions were consistently thicker than in the hI-con1–treated eyes (Fig. 6). This approached yet did not reach statistical significance.

Serum Pazopanib

The calculated and expected pazopanib concentrations of 12 different spiked serum samples were compared. The calculated and expected pazopanib concentrations are similar, suggesting the suitability of the analytic method. The lower limit of quantitation for the assay was 600 pg/mL. All serum samples analyzed were below these levels. Also, background levels could be detected in control samples. Serum concentration measured was the highest in the SC pazopanib group (239 ± 65 pg/mL), followed by Ivit pazopanib (142 ± 26 pg/mL), Ivit bevacizumab (126 ± 27 pg/mL), and then vehicle controls (124 ± 40 pg/mL). However, the values were well below the effective lower limit of quantitation (600 pg/mL), and there was an interfering background signal in animals not treated with pazopanib.

Discussion

Our modified porcine model of surgically induced CNV, as originally described,[4,6] represents a reliable and reproducible model to study type 2 CNV in vivo. Our results demonstrate consistent type 2 CNV induction, similar to the lesion type

Investigative Ophthalmology & Visual Science

found in some cases of human AMD. However, all animal models of human disease have limitations. There are documented advantages of this methodology over the induction of CNV with laser. In fact, our attempts to replicate laser-induced CNV in the pig resulted in a very low rate of CNV induction and a very high rate of CNV involution when compared to the nearly 100% CNV induction using the surgical model. Additionally, the surgery is thought to involve less retinal injury than the laser models.[5] Most CNV lesion types in human AMD are classified as either type 1 CNV, located between Bruch's membrane and the RPE, or polypoidal choroidal vasculopathy. The frequency of occurrence varies with genetic background.[38] The CNV lesion type frequencies found in the clinical setting, based on fluorescein angiographic definitions of classic, occult, or predominantly classic, suggest that the majority of lesions found in human AMD cases are subfoveal and occult, or mixed lesions, most consistent with type 1 CNV.[39] Despite these differences in lesion type, we feel that the pig model allows effective analysis of the pharmacodynamics of exudative AMD. A key advantage is the reproducibility of the CNV complex that allows for direct size comparisons, especially lesion height. However, a key limitation is the scarring and inflammatory nature of our induced lesions that may create an altered state from the lesions that result from aging. Also, type 1 CNV is likely due to aging and a more gradual deterioration in the integrity of Bruch's membrane. Aging is difficult to reproduce in an animal model.

Most of the measured differences in CNV lesion size in the pig model depend upon lesion height. This model relies on mechanical breaks in Bruch's membrane, and the subsequent CNV lesion diameter (X and Y dimensions) can vary based on the number and distribution of punctures during surgical induction. For this reason, we attempted to match the size of the punctures with the optic nerve of the animal. Also, prior studies have documented the time course of CNV progression, beginning with enucleation 30 minutes (essentially time zero), post induction, to 3, 7, 14, 28, and 42 days. In our study, drug delivery was masked and randomly assigned after induction of the CNV, thus minimizing the chances for bias. In fact, there were no significant differences in lesion diameters or surface area in any of the control or treatment groups. Thus, we believe that the consistency of horizontal lesion size is important to allow for a reliable comparison between groups. For treatment effect, we rely more on lesion height as a primary indicator of antiangiogenesis.

In our study, we found that Ivit pazopanib had a statistically significant reduction of CNV height with a trend, yet not statistically significant, of thinner lesions in eyes treated with Ivit bevacizumab and hI-con1. Since each of these agent's mechanism of action differs, translating the results back to humans may also require further analysis. We suspect that the humanized antibody to VEGF may not perform as well in porcine CNV as it does in humans. Also, the number of cases for comparison (especially with hI-con1, $n = 4$) may be too small to determine a meaningful difference. In fact, while Lassota et al.[2,40] found less fluorescein leakage of surgically induced CNV treated with bevacizumab, the lesion sizes were no different from controls. Iandiev et al.[41] studied the effect of bevacizumab in the live pig model and measured a decrease in the transcriptional expression of VEGF-A. However, their model did not include induction of CNV.

Pazopanib's mechanism of action[42] to inhibit both VEGF pathways and PDGFR-B, along with its low solubility, combine to make pazopanib an excellent candidate for sustained delivery. We propose that this drug's multifactorial mechanism of action makes it a potent inhibitor of CNV. Also, the low solubility may enable a prolonged treatment effect, and such an effect may differ from biologic antibodies that target these same pathways and are currently in human clinical trials.[43] Thus, pazopanib has ideal physical properties conducive to studying this agent in the SCS. In fact, triamcinolone acetonide has similar physical properties and was found to be an excellent compound for effective delivery in the SCS (long-term action, low systemic levels).[20]

The Ivit route of pazopanib delivery demonstrated a meaningful inhibition of CNV lesion height in our model while the SC delivery did not. There may be several reasons for this difference. First, the location of the CNV is posterior, and the SC pazopanib was delivered 6 mm posterior to the limbus. While drugs may spread throughout the SCS, we did not measure this distribution, and perhaps the diffusional kinetics limit the amount of drug reaching the area centralis of the pig eye. Second, the slow dissolution of the drug may have been insufficient to allow adequate therapeutic levels to diffuse effectively from the location of delivery to the area centralis. Third, by avoiding the choroid blood flow, Ivit pazopanib may have a more sustained presence in the eye and especially at the area centralis. Fourth, it is possible that the outer choroid blood flow, transscleral diffusion, or uveoscleral outflow channels may act as a diffusional barrier to pazopanib reaching the inner choroid from the SCS. However, we do not believe that the total SC dose was insufficient, as the Ivit route appeared to be efficacious. Nevertheless, the low solubility of the pazopanib suspension could have led to underdosing as the larger, particulate material was retained in the eddy currents of the syringe, thus leading to an unexpected dosing variation. Following each SC injection, we were unable to confirm the amount of pazopanib in the resultant SC bleb or how much of the drug diffused posteriorly toward the area centralis. Also, we were unable to directly compare the systemic levels between the two delivery routes due to the limit of quantitation. Finally, the role of postvitrectomy pharmacokinetics should be considered and may be substantially different in this model.[44]

The hI-con1 delivery was via the Ivit route, and the proposed mechanism of action is to induce regression of CNV.[36] Thus, in our model, we delayed the Ivit injection of this agent until 2 weeks after CNV induction. We found a reduction in lesion area in the CNV using this agent, yet were unable to confirm the proposed NK-mediated regression of CNV with Ivit hI-con1.[45] It is possible that our immune markers were not specific for porcine NK cells. Tezel et al.[36] previously demonstrated a dramatic reduction in CNV lesion size in laser-induced CNV in the pig model. However, when we attempted the laser-induced CNV in our model, we found rapid involution of CNV in the controls as well as the treated eyes. In fact, we had difficulties finding histologic evidence of CNV at week 2 post induction and felt that the healthy RPE of the pig eye induces rapid, spontaneous involution of CNV. Therefore, we had a much more robust CNV induction using the surgical model[3] in our studies.

We were not able to confirm the proposed mechanism of action of hI-con1. A possible explanation for not identifying NK cells is that the mechanism of CNV regression occurred prior to the time of enucleation and our specimens were obtained after the involvement of the NK cells. We intentionally delayed delivery of hI-con1 until 14 days post CNV induction. Thus, by examining the CNV lesions 1 to 2 weeks after drug delivery, we may have missed the presence of NK cell–mediated mechanistic window. Another possible explanation is that the humanized antibody with a human Fc domain may have less affinity for NK cells in our pig CNV model. Nevertheless, there was a reduction of the lesion size of hI-con1–treated animals as compared to controls.

We found that SC drug delivery using the microneedles was very simple to administer and had technical requirements

equivalent to a standard Ivit injection. Our study was not designed as a pharmacokinetic analysis of tissue drug levels. We believe that the location of the drug depot in the SCS is likely to be an important variable. SC drug deposition is expected to persist longer with greater doses, similar to the Ivit route, due to dissolution.[46]

We have been successful in generating type 2 CNV in pigs that is highly reproducible in nearly all cases. Additionally, the globe size, blood flow patterns, RPE, and other anatomic and physiological similarities between the pig and human eyes make the pig model an excellent pharmacodynamic, preclinical system to study antiangiogenesis. The CNV size may vary, based on wound construction and the healing response. In using this model, all attempts should be made to create similar, reproducible lesions. Obviously, there are other inevitable variations in surgical procedures, such as the amount and degree of RPE debridement. The number of animals studied, combined with masked random assignments, should minimize bias and optimize the reliability of this model. The histopathologic analysis of the CNV was also performed in a masked fashion to further minimize possible bias. Finally, the consistent and reproducible induction of CNV in the porcine model creates reliable horizontal dimensions of the CNV. Thus, the height measure is the most relevant measure of treatment efficacy.

In summary, we have found that Ivit pazopanib inhibits surgically induced CNV lesion size in the pig model when compared to vehicle controls and warrants further studying. CNV inhibition using either Ivit hI-con1 (strong trend) or SC pazopanib did not reach statistical significance. The SC route remains a viable route for further study. Optimizing the drug depot locations, developing better sustained-release formulations, and identifying new and novel anti-aging agents all remain worthy goals for further alleviating the current burden of treating age-related macular disease.

Acknowledgments

Supported in part by National Institutes of Health/National Eye Institute RO1 EY022097, P30 EY006360 (Department Core Grant), the Georgia Research Alliance, and an unrestricted grant from Research to Prevent Blindness to the Department of Ophthalmology at Emory University.

Disclosure: **J. Tran**, None; **C. Craven**, None; **K. Wabner**, None; **J. Schmit**, None; **B. Matter**, None; **U. Kompella**, None; **H.E. Grossniklaus**, None; **T.W. Olsen**, iMacular Regeneration LLC (S)

References

1. Sorensen NB, Lassota N, Kyhn MV, et al. Functional recovery after experimental RPE debridement, mfERG studies in a porcine model. *Graefes Arch Clin Exp Ophthalmol*. 2013; 251:2319–2325.
2. Lassota N, Prause JU, Scherfig E, Kiilgaard JF, la Cour M. Clinical and histological findings after intravitreal injection of bevacizumab (Avastin) in a porcine model of choroidal neovascularization. *Acta Ophthalmol*. 2010;88:300–308.
3. Lassota N, Kiilgaard JF, la Cour M, Scherfig E, Prause JU. Natural history of choroidal neovascularization after surgical induction in an animal model. *Acta Ophthalmol*. 2008;86: 495–503.
4. Lassota N, Kiilgaard JF, Prause JU, Qvortrup K, Scherfig E, la Cour M. Surgical induction of choroidal neovascularization in a porcine model. *Graefes Arch Clin Exp Ophthalmol*. 2007; 245:1189–1198.
5. Lassota N, Kiilgaard JF, Prause JU, la Cour M. Correlation between clinical and histological features in a pig model of choroidal neovascularization. *Graefes Arch Clin Exp Ophthalmol*. 2006;244:394–398.
6. Kiilgaard JF, Andersen MV, Wiencke AK, et al. A new animal model of choroidal neovascularization. *Acta Ophthalmol Scand*. 2005;83:697–704.
7. Wong WL, Su X, Li X, et al. Global prevalence of age-related macular degeneration and disease burden projection for 2020 and 2040: a systematic review and meta-analysis. *Lancet Glob Health*. 2014;2:e106–e116.
8. Patel SR, Lin ASP, Edelhauser HF, et al. Suprachoroidal drug delivery to the back of the eye using hollow microneedles. *Pharm Res*. 2011;1:166–176.
9. Olsen TW, Sanderson S, Feng X, Hubbard WC. Porcine sclera: thickness and surface area. *Invest Ophthalmol Vis Sci*. 2002; 43:2529–2532.
10. Brown DM, Kaiser PK, Michels M, et al. Ranibizumab versus verteporfin for neovascular age-related macular degeneration. *N Engl J Med*. 2006;355:1432–1444.
11. The CATT Research Group. Ranibizumab and bevacizumab for neovascular age-related macular degeneration. *N Engl J Med*. 2011;364:1897–1908.
12. Rich RM, Rosenfeld PJ, Puliafito CA, et al. Short-term safety and efficacy of intravitreal bevacizumab (Avastin) for neovascular age-related macular degeneration. *Retina*. 2006;26:495–511.
13. Rosenfeld PJ, Brown D, Heier JS, et al. Ranibizumab for neovascular age-related macular degeneration. *N Engl J Med*. 2006;355:1419–1431.
14. Gohil R, Crosby-Nwaobi R, Forbes A, Burton B, Hykin P, Sivaprasad S. Caregiver burden in patients receiving ranibizumab therapy for neovascular age related macular degeneration. *PLoS One*. 2015;10:e0129361.
15. Saxena N, George PP, Hoon HB, Han LT, Onn YS. Burden of wet age-related macular degeneration and its economic implications in Singapore in the year 2030. *Ophthalmic Epidemiol*. 2016;23:232–237.
16. Sampat KM, Garg SJ. Complications of intravitreal injections. *Curr Opin Ophthalmol*. 2010;21:178–183.
17. Hasler PW, Bloch SB, Villumsen J, Fuchs J, Lund-Andersen H, Larsen M. Safety study of 38,503 intravitreal ranibizumab injections performed mainly by physicians in training and nurses in a hospital setting. *Acta Ophthalmol*. 2015;93:122–125.
18. Olsen TW, Edelhauser HF, Lim J, Geroski DH. Human scleral permeability. Effects of age, cryotherapy, transscleral diode laser, and surgical thinning. *Invest Ophthalmol Vis Sci*. 1995; 36:1893–1903.
19. Einmahl S, Savoldelli M, Hermies D, Tabatabay C, Gurny R, Behar-Cohen F. Evaluation of a novel biomaterial in the suprachoroidal space of the rabbit eye. *Invest Ophthalmol Vis Sci*. 2002;43:1533–1539.
20. Olsen TW, Feng X, Wabner K, et al. Cannulation of the suprachoroidal space: a novel drug delivery methodology to the posterior segment. *Am J Ophthalmol*. 2006;142:777–787.
21. Olsen TW, Feng X, Wabner K, Csaky K, Pambuccian S, Cameron JD. Pharmacokinetics of pars plana intravitreal injections versus microcannula suprachoroidal injections of bevacizumab in a porcine model. *Invest Ophthalmol Vis Sci*. 2011;52:4749–4756.
22. Gilger BC, Abarca EM, Salmon JH, Patel S. Treatment of acute posterior uveitis in a porcine model by injection of triamcinolone acetonide into the suprachoroidal space using microneedles. *Invest Ophthalmol Vis Sci*. 2013;54:2483–2492.
23. Olsen TW, Feng X, Wabner K, Csaky K, Pambuccian S, Cameron JD. Pharmacokinetics of pars plana intravitreal injections versus microcannula suprachoroidal injections of

bevacizumab in a porcine model. *Invest Ophthalmol Vis Sci*. 2011;52:4749–4756.

24. Patel SR, Berezovsky DE, McCarey BE, Zarnitsyn V, Edelhauser HF, Prausnitz MR. Targeted administration into the suprachoroidal space using a microneedle for drug delivery to the posterior segment of the eye. *Invest Ophthalmol Vis Sci*. 2012;53:4433–4441.
25. Patel SR, Lin ASP, Edelhauser HF, Prausnitz MR. Suprachoroidal drug delivery to the back of the eye using hollow microneedles. *Pharm Res*. 2011;28:166–176.
26. Jo N, Mailhos C, Ju M, et al. Inhibition of platelet-derived growth factor B signaling enhances the efficacy of anti-vascular endothelial growth factor therapy in multiple models of ocular neovascularization. *Am J Pathol*. 2006;168:2036–2053.
27. Kumar R, Knick VB, Rudolph SK, et al. Pharmacokinetic-pharmacodynamic correlation from mouse to human with pazopanib, a multikinase angiogenesis inhibitor with potent antitumor and antiangiogenic activity. *Mol Cancer Ther*. 2007;6:2012–2021.
28. Takahashi K, Saishin Y, Saishin Y, King AG, Levin R, Campochiaro PA. Suppression and regression of choroidal neovascularization by the multitargeted kinase inhibitor pazopanib. *Arch Ophthalmol*. 2009;127:494–499.
29. Danis R, McLaughlin MM, Tolentino M, et al. Pazopanib eye drops: a randomised trial in neovascular age-related macular degeneration. *Br J Ophthalmol*. 2014;98:172–178.
30. Singh R, Wurzelmann JI, Ye L, et al. Clinical evaluation of pazopanib eye drops in healthy subjects and in subjects with neovascular age-related macular degeneration. *Retina*. 2014;34:1787–1795.
31. Hu Z, Garen A. Intratumoral injection of adenoviral vectors encoding tumor-targeted immunoconjugates for cancer immunotherapy. *Proc Natl Acad Sci U S A*. 2000;97:9221–9225.
32. Wang B, Chen YB, Ayalon O, Bender J, Garen A. Human single-chain Fv immunoconjugates targeted to a melanoma-associated chondroitin sulfate proteoglycan mediate specific lysis of human melanoma cells by natural killer cells and complement. *Proc Natl Acad Sci U S A*. 1999;96:1627–1632.
33. Hu Z, Garen A. Targeting tissue factor on tumor vascular endothelial cells and tumor cells for immunotherapy in mouse models of prostatic cancer. *Proc Natl Acad Sci U S A*. 2001;98:12180–12185.
34. Contrino J, Hair G, Kreutzer DL, Rickles FR. In situ detection of tissue factor in vascular endothelial cells: correlation with the malignant phenotype of human breast disease. *Nat Med*. 1996;2:209–215.
35. Bora PS, Hu Z, Tezel TH, et al. Immunotherapy for choroidal neovascularization in a laser-induced mouse model simulating exudative (wet) macular degeneration. *Proc Natl Acad Sci U S A*. 2003;100:2679–2684.
36. Tezel TH, Bodek E, Sonmez K, et al. Targeting tissue factor for immunotherapy of choroidal neovascularization by intravitreal delivery of factor VII-Fc chimeric antibody. *Ocul Immunol Inflamm*. 2007;15:3–10.
37. Olsen TW, Bottini AR, Mendoza P, Grossniklaus HE. The age-related macular degeneration complex: linking epidemiology and histopathology using the Minnesota Grading System (The Inaugural Frederick Blodi Lecture). *Trans Am Ophthalmol Soc*. 2015;113:3–9.
38. Miyake M, Tsujikawa A, Yamashiro K, et al. Choroidal neovascularization in eyes with choroidal vascular hyperpermeability. *Invest Ophthalmol Vis Sci*. 2014;55:3223–3230.
39. Olsen TW, Feng X, Kasper TJ, Rath PP, Steuer ER. Fluorescein angiographic lesion type frequency in neovascular age-related macular degeneration. *Ophthalmology*. 2004;111:250–255.
40. Lassota N. Clinical and histological aspects of CNV formation: studies in an animal model. *Acta Ophthalmol*. 2008;86(thesis 2):1–28.
41. Iandiev I, Francke M, Makarov F, et al. Effects of intravitreal bevacizumab (Avastin) on the porcine retina. *Graefes Arch Clin Exp Ophthalmol*. 2011;249:1821–1829.
42. Schutz FA, Choueiri TK, Sternberg CN. Pazopanib: clinical development of a potent anti-angiogenic drug. *Crit Rev Oncol Hematol*. 2011;77:163–171.
43. Jaffe GJ, Ciulla TA, Ciardella AP, et al. Dual antagonism of PDGF and VEGF in neovascular age-related macular degeneration: a phase IIb, multicenter, randomized controlled trial. *Ophthalmology*. 2017;124:224–234.
44. Xu Y, You Y, Du W, et al. Ocular pharmacokinetics of bevacizumab in vitrectomized eyes with silicone oil tamponade. *Invest Ophthalmol Vis Sci*. 2012;53:5221–5226.
45. Hu Z, Li J. Natural killer cells are crucial for the efficacy of Icon (factor VII/human IgG1 Fc) immunotherapy in human tongue cancer. *BMC Immunol*. 2010;11:49.
46. Durairaj C, Kim SJ, Edelhauser HF, Shah JC, Kompella UB. Influence of dosage form on the intravitreal pharmacokinetics of diclofenac. *Invest Ophthalmol Vis Sci*. 2009;50:4887–4897.

Investigative Ophthalmology & Visual Science